coatings

MDPI

Article

Oscillating Magnetic Drop: How to Grade Water-Repellent Surfaces

Angelica Goncalves Dos Santos [1], Francisco Javier Montes-Ruiz Cabello [2], Fernando Vereda [2], Miguel A. Cabrerizo-Vilchez [2] and Miguel A. Rodriguez-Valverde [2,*]

[1] Department of Physics, Florida State University, Tallahassee, FL 32306, USA; amg16k@my.fsu.edu
[2] Biocolloid and Fluid Physics Group, Applied Physics Department, Faculty of Sciences, University of Granada, 18071 Granada, Spain; fjmontes@ugr.es (F.J.M.-R.C.); fvereda@ugr.es (F.V.); mcabre@ugr.es (M.A.C.-V.)
* Correspondence: marodri@ugr.es; Tel.: +34-958-243-229

Received: 19 February 2019; Accepted: 17 April 2019; Published: 21 April 2019

Abstract: Evaluation of superhydrophobic (SH) surfaces based on contact angle measurements is challenging due to the high mobility of drops and the resolution limits of optical goniometry. For this reason, some alternatives to drop-shape methods have been proposed such as the damped-oscillatory motion of ferrofluid sessile drops produced by an external magnetic field. This approach provides information on surface friction (lateral/shear adhesion) from the kinetic energy dissipation of the drop. In this work, we used this method to compare the low adhesion of four commercial SH coatings (Neverwet, WX2100, Ultraever dry, Hydrobead) formed on glass substrates. As ferrofluid, we used a maghemite aqueous suspension (2% *v*/*v*) synthesized ad hoc. The rolling magnetic drop is used as a probe to explore shear solid–liquid adhesion. Additionally, drop energy dissipates due to velocity-dependent viscous stresses developed close to the solid–liquid interface. By fitting the damped harmonic oscillations, we estimated the decay time on each coating. The SH coatings were statistically different by using the mean damping time. The differences found between SH coatings could be ascribed to surface–drop adhesion (contact angle hysteresis and apparent contact area). By using this methodology, we were able to grade meaningfully the liquid-repelling properties of superhydrophobic surfaces.

Keywords: water-repellent surfaces; ferrofluid drop; magnetic field; damped harmonic oscillation

1. Introduction

Liquid-repellent surfaces are identified as surfaces with low contact angle hysteresis (<10°) and high contact angles (>150°) [1]. Hysteresis is directly related to the energy cost during the total or partial detachment of a drop from a solid surface. Preparation of superhydrophobic (SH) surfaces is well-established and their water repelling property is commonly evaluated with contact angle or critical sliding angle measurements by using optical goniometry, as happens with the tilting plate method (inclined sessile drop) [2]. However, although this method is useful to illustrate water repellency, it provides low-resolution values of contact angle or critical sliding angle for SH surfaces. The difficult localization of the contact points of non-wetting drops, the insufficient resolution for high contact angles with both the conventional optical devices and numerical fitting of drop profiles [3], the resolution of standard inclinometers working at very low tilt angles (<5°) and the monitoring of "restless" drops placed on SH surfaces [4] required to establish new methodologies. Since the high drop mobility observed on a surface reveals its liquid repellency, the kinetic energy dissipation of a moving sessile drop might quantify the surface friction due to adhesion hysteresis.

A magnetic drop can be manipulated with an external magnetic field (magneto-wetting) [5–11]. The damped-oscillatory motion of a water-based ferrofluid sessile drop driven by a fixed permanent magnet [12] might be used to evaluate experimentally, without further theoretical treatment, the water repellency of non-magnetizable SH surfaces. It is known that, on SH surfaces, a moving sessile drop really rolls, it does not slide [13]. Far from the contact region, the rolling drop moves in a similar way to a rolling rigid-solid. This way, the bulk effect of viscosity may be ignored and the viscous forces mainly act near the contact area [14]. Moreover, this viscous dissipation is further reduced on SH surfaces where the actual drop contact area is particularly low. This approach is different to the viscous forces considered by Timonen et al. [12]. Otherwise, solid–liquid adhesion friction depends on contact angle hysteresis and contact line length of the drop. In this scenario, the plausible differences found with moving drops on SH surfaces would be exclusive to the surface-drop interaction.

In this work, we compared four commercial SH coatings on glass by using the decay time of an oscillating ferrofluid drop released far from its equilibrium. We found the optimal magnetic field to minimize the drop shape distortion and to reproduce longer oscillating motions. We studied the dependence of the damping time on the surface-drop contact area and the drop volume.

2. Materials and Methods

2.1. Fabrication of Superhydrophobic Glass Samples

We evaluated four commercial superhydrophobic coatings: Neverwet Multi-Surface (RUST-OLEUM, Coventry, UK), WX-2100 (Cytonix LLC, Beltsville, MD, USA), Ultra-Ever Dry (Tap Iberica., Burjassot, Spain), and Hydrobead (Hydrobead, San Diego, CA, USA). They were sprayed on clean glass slides, as each supplier recommended. We assumed that these coatings are organic, without metal traces.

2.2. Ferrofluid Preparation

The aqueous ferrofluid was prepared at 2% *v*/*v* as described elsewhere [15,16]. The process starts with the synthesis of the magnetite nanoparticles by means of the well-known coprecipitation method. These particles are subsequently oxidized to maghemite (γ-Fe_2O_3) with $Fe(NO_3)_3$ and then functionalized with citrate. The electric charge of citrate carboxyl groups at neutral pH prevents particle aggregation. In addition, the small size of the particles (typically 10 nm) in combination to the thermal agitation make the dispersion sedimentation unlikely. As a result, the ferrofluid remains stable for months. The values of density and surface tension of the ferrofluid are 1.04 g/mL and 67.4 mN/m, respectively, which are close to those of pure water. The surface tension indicates that the magnetic nanoparticles have no significant interfacial activity.

2.3. Contact Angle Measurements

The contact angle measurements were conducted with the tilting plate method [2]. We used 100 µL drops of Milli-Q water to increase the density of metastable drop configurations separated by smaller energy barriers and the spatial resolution of the method. Drops were gently deposited at the center of the sample, which is fixed to the tilting platform, oriented horizontally. The drop placement was non-trivial because the drops rolled off the samples very easily. Once the drop was deposited and static, the platform was automatically inclined at a constant rate (5°/s). Side views of the drop were captured simultaneously at 16 fps. We measured the Advancing Contact Angle (ACA) and Receding Contact Angle values (RCA), at both sides of the profile of the deformed drop by using independent elliptical fittings [2]. From these values, we calculated the Contact Angle Hysteresis (CAH) as the difference ACA-RCA.

2.4. Oscillating Magnetic Drop Set-up

The set-up for the oscillating magnetic drop experiments is illustrated in Figure 1. Below the surface, a cylindrical NdFeB magnet with 1.20 cm-diameter and 0.53 cm-height (Supermagnete, Gottmadingen, Germany) was assembled to a vertical aluminum screw. This screw allowed for the adjustment of the surface-to-magnet distance. The magnetic field strength was measured with a teslameter (5170 Gauss/Tesla Meter, FW BELL-EuroMC, Stains, France). Once the SH coating was placed on the stage, the system was leveled out to ensure that the magnetic drop moved randomly on the surface in the absence of the external magnetic field. We deposited three ferrofluid drops with a handheld micropipette on each SH coating. We studied two volumes: 5 and 10 μL. Each drop was initially static thanks to a secondary weak magnet (0.44 cm-height) placed below the surface, at a horizontal distance of 1.76 cm from the primary magnet. The action of this secondary magnet was allowed from an adjustable stop. Once the secondary magnet was moved down, the ferrofluid drop was released, describing a damped oscillatory motion around the primary magnet. During the overall motion, we acquired side views (512 × 128 pixel, 212 pixel/cm) of the back-illuminated drop with a high-speed camera (Phantom, Miro) at 1000 fps. The geometrical drop parameters, such as centroid, contact angles, and contact radius, were calculated by elliptical fitting of each drop contour. The value of contact angle at each side of the drop contour was calculated from the corresponding slope of the best fit evaluated at the contact point (initial and final points of contour). Our resolution was enough to find meaningfully the horizontal positions of drop centroid. We measured the decay time τ of drop motion by fitting the centroid positions to a damped sine wave function ($A\exp(-t/\tau)\sin(\omega t + \varphi)$). We discarded the initial and final oscillations as suggested by Timonen et al. [12].

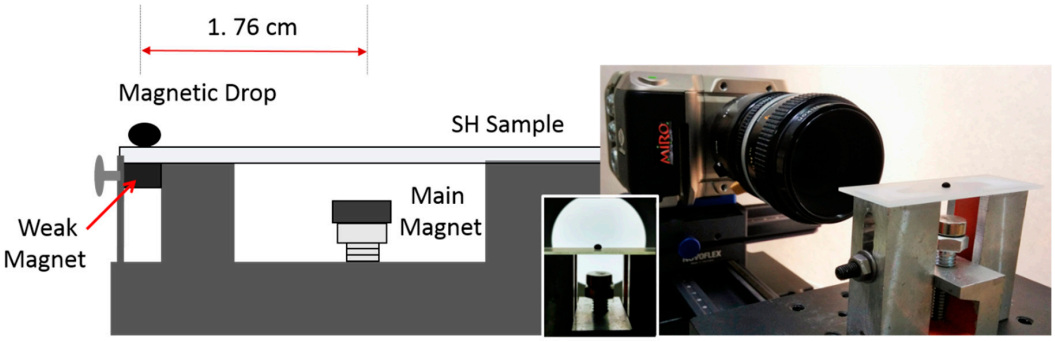

Figure 1. Set-up for oscillating magnetic drop experiments.

3. Results

3.1. Contact Angle Measurements

In Table 1, we show the ACA, RCA, and CAH values measured with the tilting plate method (100 μL-water drops) for the coatings used in this study. These values were averaged over, at least, three experiments. We identify all the coatings as superhydrophobic but no significant difference was found between them.

Table 1. Contact angles of Milli-Q water drops (100 μL) measured with the tilting plane method on the Superhydrophobic (SH) coatings. ACA: Advancing Contact Angle, RCA: Receding Contact Angle and CAH: Contact Angle Hysteresis.

Coating	ACA (°)	RCA (°)	CAH (°)
WX-2100	149 ± 2	147 ± 4	2 ± 6
Hydrobead	152 ± 1	146 ± 3	6 ± 4
Ultra-Ever-Dry	148 ± 2	146 ± 2	2 ± 4
Neverwet	151 ± 3	148 ± 3	3 ± 6

3.2. Magnetic Field Strength

We evaluated the magnetic field strength on the sample stage. This field was maximum close to the primary magnet axis, as expected. We varied the magnet-to-surface distance (r) and the results are shown in Figure 2a. The (maximum) magnetic field strength scales as $1/r$, as predicted by theory. We also measured the magnetic field strength at different distances from the primary magnet axis (d) (Figure 2b), for four surface-to-magnet distances.

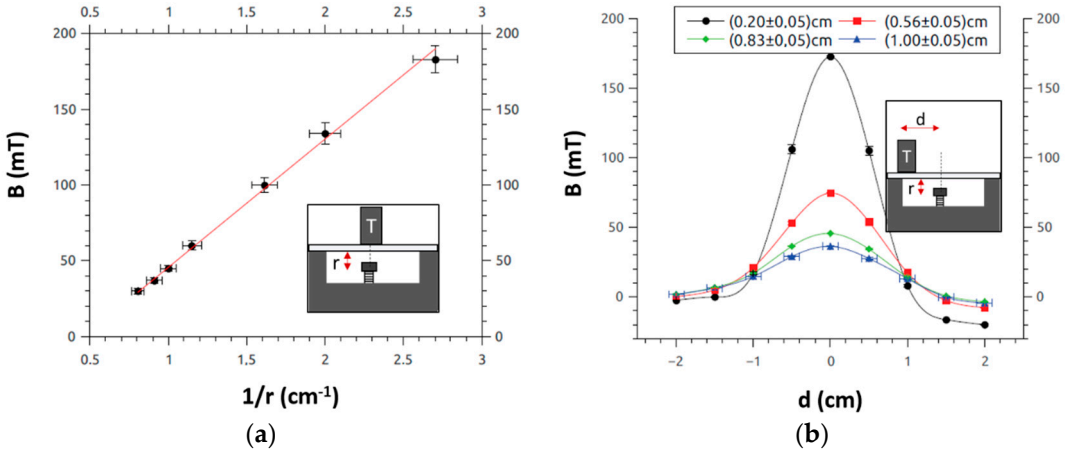

Figure 2. (**a**) Maximum magnetic field strength (measured at the magnet axis) as a function of the inverse of the surface-to-magnet distance. (**b**) Magnetic field strength at different horizontal positions on the sample stage from the magnet axis. The symbol "T" in the insets stands for the position of the Teslameter probe.

3.3. Drop Shape Distortion Induced by the Magnetic Field

Magnetic force depends on the field gradient and the ferrofluid magnetization depends on the field strength. Besides, it is known that (surface) magnetic forces alter the wetting response of magnetic drops on solids such as electric forces in electrowetting. The magnetic sessile drop is pressed against the surface by the effect of the external magnetic field, which increases the apparent wet area. We intended to find an optimal surface-to-magnet separation that balances the minimum drop shape distortion and at the same time produces a significantly damped-oscillating drop motion. In particular, we analyzed how the values of drop contact area and contact angle, averaged during the entire drop motion, were modified by the magnetic field. We monitored these parameters for oscillating 5 µL-drops over the Hydrobead coating. In Figure 3a, we show how the inverse of the average drop contact area ($1/\langle A \rangle$) scales as the surface-to-magnet distance (r). From Figure 2a, one may conclude that the contact area increases linearly with the magnetic field strength. In Figure 3b, we show how the average contact angle $\langle \theta \rangle$ decreases linearly with the average contact area ($\langle A \rangle$), as surface-to-magnet distance becomes smaller. The magnetic drop is squashed against the surface as the magnetic force (normal net force) increases, and this increases noticeably the contact area and decreases the contact angle. Short surface-to-magnet distances might produce a total or partial transition in the drop [10] from the Cassie regime (heterogeneous wetting) to the Wenzel regime (homogeneous wetting). In our experiments, for a fixed surface-to-magnet distance, the drop contact area also oscillates because the external magnetic field is not uniform on the SH coating: a greater contact area was observed close to the equilibrium position. This effect complicates the overall drop motion, with a variable period (not pure harmonic). We found that 0.96 cm was the optimal surface-to-magnet distance (peak field of 50 mT) to reproduce a significantly damped-oscillating motion of almost undistorted drops.

We fixed the surface-to-magnet distance to 0.96 cm to evaluate the shape variations of oscillating drops over the SH coatings. In Figure 4, we show the results for two representative coatings (Hydrobead and Neverwet). We plot the average dynamic contact angle (estimated by averaging the contact angles

measured at both sides of the drop profile) in terms of the instantaneous contact area, during the complete oscillating motion of three magnetic drops. This plot does not illustrate the response of contact angle hysteresis for each coating. A sessile drop in the Cassie-Baxter regime (on SH surfaces) may reach different configurations (different penetration depths into the asperities) according to the stability of each drop configuration against an external body force (size-dependent). In Table 2, we collect the values of oscillating contact area averaged during the entire drop motion on each coating. Except for Neverwet, the values of mean contact area were very similar. It is also remarkable the significant disagreement for this coating between the contact angles measured with the oscillating drop and the tilting plate method (see Table 1). This behavior will be confirmed in Section 3.4.

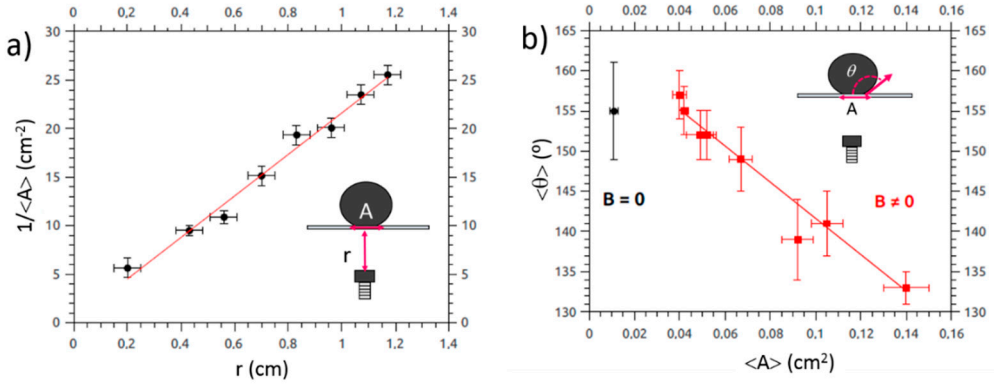

Figure 3. Shape distortion induced by the external magnetic field on an oscillating drop over a Hydrobead coating: (**a**) inverse of the average contact area versus the surface-to-magnet distance; and (**b**) the average contact angle as a function of the average contact area.

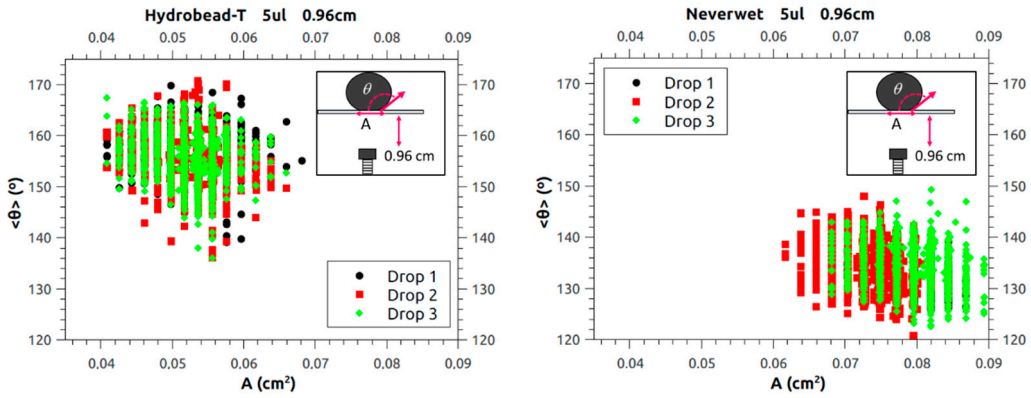

Figure 4. Average dynamic contact angle (measured at both sides of the drop) in terms of the instantaneous contact area for 5 μL-magnetic drops oscillating over glass slides coated with Hydrobead (**a**) and Neverwet (**b**). Each parameter was determined by image analysis of the single frames captured during the complete drop motion.

Table 2. Values of the mean contact area (<*A*>) during the complete drop motion (5 μL) on the SH coatings.

Coating	<*A*> (mm²)
WX-2100	5.7 ± 0.4
Hydrobead	5.2 ± 0.4
Ultra-Ever-Dry	5.1 ± 0.4
Neverwet	7.8 ± 0.4

3.4. Dynamics of Oscillating Magnetic Drops

With the surface-to-magnet distance fixed to 0.96 cm, we performed dynamic experiments based on the analysis of the motion of 5 µL-magnetic drops over each SH coating. In Figure 5, we show the evolution of the horizontal position of the drop centroid with time. In all cases, once the drop is released, it oscillates around the equilibrium position but following an underdamped motion with a decay time different for each coating. The horizontal magnetic force acts like a restorative force for horizontal distances below 1 cm respect to the equilibrium position (see Figure 2b). A moving drop on a SH surface describes a superposition of a solid rotation (producing no bulk dissipation) with a viscous friction localized in the contact area. The viscous dissipation is mainly governed by internal flows near contact area rather than in bulk. However, the energy dissipation is also caused by adhesion hysteresis. We reasonably assume that the rolling drops in our experiments undergo a synergetic dissipation due to the viscous stresses developed close to the solid–liquid interface (further reduced in SH surfaces) and the shear adhesion hysteresis. We postulate that a single exponential law, as fit model for the amplitude decay of oscillating drops, enables the capture of the dissipative effects of irreversible solid–liquid adhesion as well as velocity-dependent friction. The goodness of fit was appropriate.

We fitted the horizontal position of the drop centroid (Figure 5) to a damped-harmonic function to determine the damping time (τ). We repeated the experiments with drops of 10 µL and the results are shown in Table 3. In a simplistic scenario of velocity-dependent friction, we would expect greater drop inertia and greater damping. However, this is only found for the Neverwet coating (larger contact area). We found that the Ultra-Ever-Dry coating is the most water repellent (higher damping time), while the WX-2100 coating has the lowest repelling property (lower damping time).

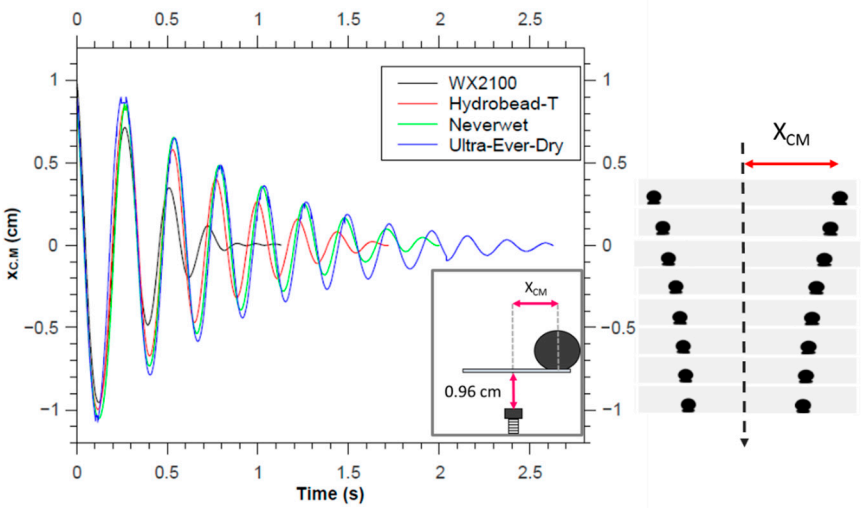

Figure 5. Damped oscillating motion of 5 µL-magnetic drops on the SH coatings, for a surface-to-magnet distance of 0.96 cm. The X_{CM} corresponds to the horizontal deviation of the drop centroid from the equilibrium (primary magnet position).

Table 3. Damping time values for oscillating magnetic drops of 5 and 10 µL on the SH coatings.

Coating	τ (s)-5 µL	τ (s)-10 µL
WX-2100	0.25 ± 0.04	0.40 ± 0.03
Hydrobead	0.61 ± 0.05	0.61 ± 0.06
Ultra-Ever-Dry	0.70 ± 0.10	0.84 ± 0.10
Neverwet	0.66 ± 0.04	0.52 ± 0.09

Like in a typical damper, the frictional force should be a function of the average contact area, but the dependence of the damping time on the size of the contact line is still unclear. We intend to explore the plausible effect of drop contact area on the damping time. In Figure 6a, we plot the

inverse of the damping time of 5 μL-magnetic drops on the Hydrobead coating versus the average contact area (modified by varying the surface-to-magnet distance). Below values of 0.1 cm^2 (low magnetic fields), the inverse of the damping time scales linearly with the average contact area of the drop. This is expected because contact angle hysteresis on rough composite surfaces depends on the fractional solid-liquid contact area [17]. However, above 0.1 cm^2, the damping time saturates due to the squashing effect on the magnetic drop, and the possible occurrence of drop configurations far from the 'fakir' state (maximum volume of air entrapped below the drop). In addition to the different wetting properties, the slope of the linear part of Figure 6a (amplified in Figure 6b) may be related to how the water-repelling properties (Cassie regime) of each coating are preserved as the magnetic drop is pressed against the surface. The drops may penetrate sufficiently into the particular surface asperities. Lower values of $1/(\tau<A>)$ for a fixed drop volume would point out to more stable configurations of drop within a well-established Cassie regime because the damping time would be less sensitive to wet area changes. In Table 4, we show the values of the slope $1/(\tau<A>)$ for each coating. This analysis was carried out for drops of 5 and 10 μL. Larger drops typically attain a more stable Cassie configuration. Instead, we observed that the values of $1/(\tau<A>)$ for the Neverwet coating were very similar for both drop volumes. The magnetic force nearly altered the incomplete hybrid wetting regime developed in this coating. In the rest of coatings, the Ultra-Ever-Dry coating was the most stable. This suggest that the Cassie regimen reproduced would be more robust, independent of the drop size.

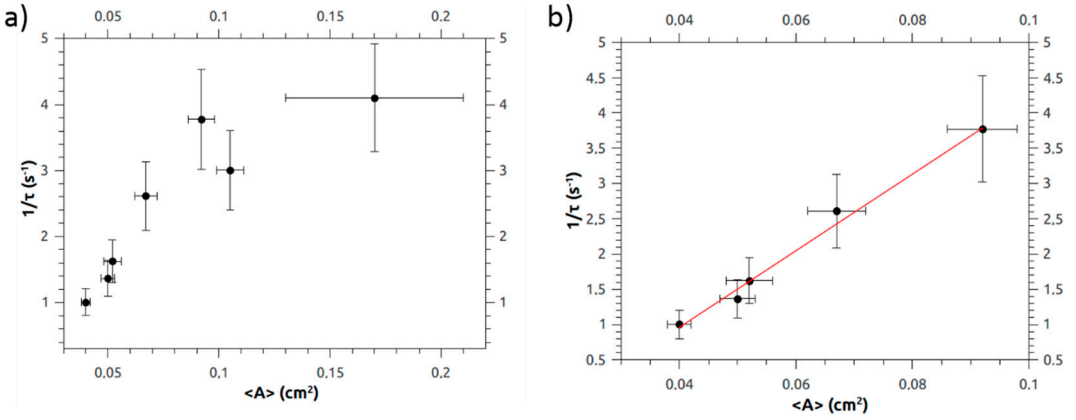

Figure 6. (**a**) Inverse of the damping time ($1/\tau$) of 5 μL-magnetic drops versus the average contact area ($<A>$), changed through the external magnetic field, on the Hydrobead coating. (**b**) Linear fit to the section of the same curve corresponding to low average areas (small fields, large surface-to-magnet distances).

Table 4. Values of $1/(\tau<A>)$ (cm^{-2} s^{-1}) corresponding to 5 and 10 μL for the SH coatings.

Coating	$1/(\tau<A>)$ (cm^{-2} s^{-1})-5 μL	$1/(\tau<A>)$ (cm^{-2} s^{-1})-10 μL
WX-2100	70 ± 16	33 ± 7
Hydrobead	32 ± 5	23 ± 9
Ultra-Ever-Dry	28 ± 6	17 ± 3
Neverwet	19 ± 2	19 ± 5

4. Discussion

Direct contact angle and hysteresis measurements of large drops (100 μL) showed that all the coatings were superhydrophobic, but this methodology was unable to identify the more efficient coating. Furthermore, the mapping of average contact angle of small drops (5 μL) in motion in terms of their contact area evidenced the contact angle hysteresis of each surface, but it did not resolve the corresponding water-repelling property. Instead, we were able to grade meaningfully non-magnetizable superhydrophobic surfaces by using the damping time of oscillating magnetic

drops ruled by the solid–liquid shear adhesion. We confirmed that this method is more sensitive than goniometry-based methods to validate superhydrophobic surfaces. We recommend using small drops (5–10 μL) of dilute aqueous ferrofluids (2% *v*/*v*). Moreover, an intense magnetic field (peak value of 50 mT) is recommended to produce a damped oscillating motion with minor changes in the average contact area and contact angle of the drop as compared to the magnetic field-off case. Further work should be addressed to explore the relationship between the damping time of water-repellent surfaces and their contact angle hysteresis, measured with force-based techniques.

Author Contributions: Conceptualization, M.A.R.V. and M.A.C.-V; Methodology, A.G.D.S., F.V. and F.J.M.-R.C.; Writing—Original Draft Preparation, M.A.R.V. and F.J.M.-R.C.; Writing—Review and Editing, M.A.R.V. and F.J.M.-R.C.; Supervision, M.A.R.V. and M.A.C.-V.; Project Administration, M.A.R.V and M.A.C.-V.; Funding Acquisition, M.R.V. and M.A.C.-V.

Funding: This research was financed by the State Research Agency (SRA) and European Regional Development Fund (ERDF) through the project MAT2017-82182-R. Fernando Vereda acknowledges financial support from MAT 2016-78778-R and PCIN-2015-051 projects (Spain).

Acknowledgments: We acknowledge Juan de Vicente (UGR) for the assistance in the measurements of magnetic field strength with teslameter.

Conflicts of Interest: The authors declare no conflict of interest.

References

1. Lv, X.; Tian, D.; Peng, Y.; Li, J.; Jiang, G. Superhydrophobic magnetic reduced graphene oxide-decorated foam for efficient and repeatable oil-water separation. *Appl. Surf. Sci.* **2019**, *466*, 937–945. [CrossRef]
2. Ruiz-Cabello, F.J.M.; Rodriguez-Valverde, M.A.; Cabrerizo-Vilchez, M. A new method for evaluating the most stable contact angle using tilting plate experiments. *Soft Matter* **2011**, *7*, 10457–10461. [CrossRef]
3. Srinivasan, S.; McKinley, G.H.; Cohen, R.E. Assessing the accuracy of contact angle measurements for sessile drops on liquid-repellent surfaces. *Langmuir* **2011**, *27*, 13582–13589. [CrossRef] [PubMed]
4. Tian, X.; Verho, T.; Ras, R.H.A. Moving superhydrophobic surfaces toward real-world applications. *Science* **2016**, *352*, 142–143. [CrossRef] [PubMed]
5. Bormashenko, E.; Pogreb, R.; Bormashenko, Y.; Musin, A.; Stein, T. New investigations on ferrofluidics: Ferrofluidic marbles and magnetic-field-driven drops on superhydrophobic surfaces. *Langmuir* **2008**, *24*, 12119–12122. [CrossRef] [PubMed]
6. Nguyen, N.-T.; Zhu, G.; Chua, Y.-C.; Phan, V.-N.; Tan, S.-H. Magnetowetting and sliding motion of a sessile ferrofluid droplet in the presence of a permanent magnet. *Langmuir* **2010**, *26*, 12553–12559. [CrossRef] [PubMed]
7. Zhou, Q.; Ristenpart, W.D.; Stroeve, P. Magnetically induced decrease in droplet contact angle on nanostructured surfaces. *Langmuir* **2011**, *27*, 11747–11751. [CrossRef] [PubMed]
8. Zhu, G.-P.; Nguyen, N.-T.; Ramanujan, R.V.; Huang, X.-Y. Nonlinear deformation of a ferrofluid droplet in a uniform magnetic field. *Langmuir* **2011**, *27*, 14834–14841. [CrossRef] [PubMed]
9. Cheng, Z.; Lai, H.; Zhang, N.; Sun, K.; Jiang, L. Magnetically induced reversible transition between cassie and wenzel states of superparamagnetic microdroplets on highly hydrophobic silicon surface. *J. Phys. Chem. C* **2012**, *116*, 18796–18802. [CrossRef]
10. Nguyen, N.-T. Deformation of ferrofluid marbles in the presence of a permanent magnet. *Langmuir* **2013**, *29*, 13982–13989. [CrossRef] [PubMed]
11. Manukyan, S.; Schneider, M. Experimental investigation of wetting with magnetic fluids. *Langmuir* **2016**, *32*, 5135–5140. [CrossRef] [PubMed]
12. Timonen, J.V.I.; Latikka, M.; Ikkala, O.; Ras, R.H.A. Free-decay and resonant methods for investigating the fundamental limit of superhydrophobicity. *Nat. Commun.* **2013**, *4*, 2398. [CrossRef] [PubMed]
13. Schellenberger, F.; Encinas, N.; Vollmer, D.; Butt, H.-J. How water advances on superhydrophobic surfaces. *Phys. Rev. Lett.* **2016**, *116*, 096101. [CrossRef] [PubMed]
14. Mahadevan, L.; Pomeau, Y. Rolling droplets. *Phys. Fluids* **1999**, *11*, 2449–2453. [CrossRef]
15. Ménager, C.; Sandre, O.; Mangili, J.; Cabuil, V. Preparation and swelling of hydrophilic magnetic microgels. *Polymer* **2004**, *45*, 2475–2481. [CrossRef]

16. Aldana, S.; Vereda, F.; Hidalgo-Alvarez, R.; de Vicente, J. Facile synthesis of magnetic agarose microfibers by directed self-assembly in W/O emulsions. *Polymer* **2016**, *93*, 61–64. [CrossRef]
17. Nosonovsky, M. Model for solid-liquid and solid-solid friction of rough surfaces with adhesion hysteresis. *J. Chem. Phys.* **2007**, *126*, 224701. [CrossRef] [PubMed]